JOURNAL OF MATERIALS SCIENCE 19 (1984) 3702–3712

The effect of microcracking upon the Poisson's ratio for brittle materials

E. D. CASE
Materials and Molecular Research Division, Lawrence Berkeley Laboratory, and Department of Materials Science and Mineral Engineering, University of California, Berkeley, California 94720, USA

Microcracking–elasticity theories typically relate a decrement in elastic moduli to the number density, N, and the mean microcrack radius $\langle a \rangle$. In this paper, four microcracking–modulus theories are rewritten in terms of the macroscopic, observable parameters of Young's modulus and Poisson's ratio, eliminating the specific dependence on the difficult to measure, microscopic quantities N and $\langle a \rangle$. The rewritten microcracking elasticity theories are then compared to elasticity data on a variety of microcracked, polycrystalline ceramics.

1. Introduction

The elastic moduli of a body can be significantly affected by microcracks [1–8]. In extreme cases, the Young's modulus may drop to 10 or 20% of that observed for the nonmicrocracked material [1, 5–8]. There are a number of theories that relate the mean microcrack radius, $\langle a \rangle$, and the number density, N, of microcracks to changes in elastic moduli. However, the microscopic parameters $\langle a \rangle$ and N are difficult to determine experimentally. In this paper, it is shown that the results for each of four such theories can be rewritten in terms of the macroscopic variables of Young's modulus, Y, and Poisson's ratio, ν, eliminating the explicit dependence on the microscopic quantities N and $\langle a \rangle$. These results are compared to available data on several ceramic oxides. In addition, the difficulties in making experimental measurements of $\langle a \rangle$ and N are briefly discussed.

The geophysics literature contains a number of examples of an apparent correlation between changes in Young's, shear, or bulk modulus and changes in Poisson's ratio. In 1933, Zisman [9] noted that for a variety of naturally occurring rocks, those with a high Young's modulus commonly had a high Poisson's ratio, while rocks with a low Young's modulus commonly had a low Poisson's ratio. For rocks with initially low values of Young's modulus, Y, and Poisson's ratio, ν, Zisman found that uniaxial compression increased both Y and ν. On the other hand, if both Y and ν were initially high, then uniaxial compression had little effect on either Y or ν. For example, an increase in compressive stress from 112 to 560 kPa changed the ν of Vermont Marble from 0.142 to 0.209, while Y increased from 38.3 to 49.5 GPa. However, the same initial and final stress states for a diabase specimen left both ν and Y essentially unchanged. As an explanation of this phenomenon, Zisman suggested that compression might close cracks in the rocks, resulting in a significant increase in the elastic constants measured under stress compared to those measured under lower stress.

More recent work by Walsh includes similar data on the effect of pressure on the Poisson's ratio of Westerly granite [10]. It is now widely accepted in the geophysical literature that the closing of cracks as a function of pressure can significantly alter the mechanical, thermal, and electromagnetic properties of rocks [10–21].

Pressure is just one parameter that can affect the number or size of microcracks in a brittle material. In ceramics, it has been shown that both grain size and thermal cycling can modify the crack population [1–8]. For ceramics, there has been relatively little investigation of the effect of microcrack number density on Poisson's ratio.

0022–2461/84 $03.00 + .12

More importantly, there has been no direct comparison of elasticity data for microcracked materials with the various models that attempt to predict how the bulk elastic constants change as a function of the microcracking state. This paper shows that the observed simultaneous decrease in Young's modulus and Poisson's ratio (that results from microcracking) is in general agreement with theoretical predictions.

2. Experimental procedure

All specimens were prepared from high purity powders. No second phases were observed in as-fired specimens of Al_2O_3 [8, 22, 23], Nb_2O_5 [6, 7], Eu_2O_3 [2], or HfO_2 [24, 25], to within the resolution of X-ray diffraction. However, small amounts of MgO and Y_2O_3 are present in the $YMg_xCr_{1-x}O_3$ specimens [26].

All elasticity measurements were done by the sonic resonance technique [27–29]. The flexural and torsional frequencies of the prismatic specimens were used to calculate the Young's and shear moduli, according to the theory developed by Pickett [30] and Hasselman [31]. Equation 1 was used to compute Poisson's ratio, ν' from the measured Young's modulus, Y, and shear modulus, G.

$$\nu = \frac{Y}{2G} - 1 \tag{1}$$

The data discussed here for Al_2O_3, Gd_2O_3, HfO_2 and $YMg_xCr_{1-x}O_3$ were taken in room air, at approximately 23° C and atmospheric pressure. The measurements on Nb_2O_5 and Eu_2O_3 were done as a function of temperature in a carbon resistance furnace at a pressure of less than 5×10^{-5} torr [2, 6, 7].

The experimental uncertainties involved in sonic resonance measurements of Young's moduli and Poisson's ratio are about ± 1% and ± 10%, respectively [32, 33].

3. Results and Discussion

3.1. Description of the microcrack–elasticity theories

Walsh [10] was one of the first to model the changes in elastic moduli that occur in response to changes in the microcrack population within a specimen. Assuming a homogenous, isotropic body with a crack number density of N cracks per unit volume, the effective Poisson's ratio, ν, for the cracked body was given by Walsh as

$$\nu = \nu_0 \left(1 - \frac{4\pi}{3} N a^3\right) \tag{2a}$$

where ν_0 is the Poisson's ratio of the uncracked body, and $2a$ is the average length of the crack. In terms of the effective modulus, Y, of the cracked and Y_0, the Young's modulus of the uncracked body, Walsh found the simple linear relation

$$\nu = (Y/Y_0)\nu_0 \quad \text{or} \quad Y = Y_0(\nu/\nu_0). \tag{2b}$$

Three later theories that extend Walsh's results are those by Salganik [17, 18] and by Budiansky and O'Connell [19] and by Hasselman and Singh [34]. As the work by Hasselman is a modification of the Salganik theory, henceforth this work will be referred to as the Hasselman–Salganik theory. As was the case for Walsh's model, each of the later models treats a homogeneous, isotropic body with a number density N of randomly oriented, circular cracks* of mean radius $\langle a \rangle$. It should be noted that while Walsh's model ignores crack interactions, the other three theories attempt to treat at least first-order interactions between cracks.

For Y, Y_0, $\langle a \rangle$, ν, ν_0, and N defined as above, Salganik gives the relations

$$Y = Y_0 \left[1 - \frac{16(10 - 3\nu_0)(1 - \nu_0^2)N\langle a \rangle^3}{45(2 - \nu_0)}\right] \tag{3a}$$

$$\nu = \nu_0 \left[1 - \frac{16(3 - \nu_0)(1 - \nu_0^2)N\langle a \rangle^3}{15(2 - \nu_0)}\right] \tag{3b}$$

while Budiansky and O'Connell give

$$Y = Y_0 \left[1 - \frac{16(1 - \nu^2)(10 - 3\nu)\epsilon}{45(2 - \nu)}\right], \tag{4a}$$

where the parameter ϵ is given by

$$\epsilon = N\langle a \rangle^3 = \frac{45(\nu_0 - \nu)(2 - \nu)}{16(1 - \nu^2)[10\nu_0 - (1 + 3\nu_0)]}. \tag{4b}$$

Hasselman modified Salganik's relations to obtain†

*Salganik and Hasselman–Salganik treat only the case of circular cracks. Budiansky and O'Connell treat elliptical and rectangular cracks, with circular cracks being a special case of the elliptical cracks.

†Although no derivation is presented for the Hasselman–Salganik equations [34], one can pass from the Salganik equations to the Hasselman–Salganik relation by considering the form of the summation of a geometric series. That is, $1 - X + X^2 - + \ldots = (1 + X)^{-1}$ for $X < 1$, and for X sufficiently small, $1 - X \simeq (1 + X)^{-1}$.

$$Y = Y_0\left[1 + \frac{16(10 - 3\nu_0)(1 - \nu_0^2)N\langle a\rangle^3}{45(2 - \nu_0)}\right]^{-1} \quad (5a)$$

$$\nu = \nu_0\left[1 + \frac{16(3 - \nu_0)(1 - \nu_0^2)N\langle a\rangle^3}{15(2 - \nu_0)}\right]^{-1}. \quad (5b)$$

3.2. Recasting the theories in terms of macroscopic variables only

The expressions of Budiansky and O'Connell, Salganik, and Hasselman–Salganik can all be rewritten without explicit dependence on N or $\langle a\rangle$. For the Budiansky and O'Connell model, merely substituting equation 4b into 4a gives

$$Y = Y_0\left[1 - \frac{(\nu_0 - \nu)(10 \quad 3\nu)}{[10\nu_0 - \nu(1 + 3\nu_0)]}\right]. \quad (6)$$

For the Salganik Equations 3a and 3b, if one makes the ansatz

$$A_s = \frac{16(3 - \nu_0)(1 - \nu_0^2)N\langle a\rangle^3}{15(2 - \nu_0)}, \quad (7)$$

then substituion of Equation 7 into Equation 3b gives, upon solving for A_s,

$$A_s = \left(\frac{\nu_0 - \nu}{\nu_0}\right). \quad (8)$$

Using Equations 7 and 8, Equation 3a may then be rewritten as

$$Y = Y_0\left[1 - \frac{(10 - 3\nu_0)(\nu_0 - \nu)}{3(3 - \nu_0)\nu_0}\right]. \quad (9)$$

Using the same ansatz as above yields Equation 10 from the Hasselman–Salganik equations:

$$Y = Y_0\left[1 + \frac{(10 - 3\nu_0)(\nu_0 - \nu)}{3(3 - \nu_0)\nu}\right]^{-1}. \quad (10)$$

Equations 2b, 6, 9 and 10 thus represent the results of the four modulus decrement–microcracking theories, but rewritten in terms of the macroscopic variables Y and ν only. For convenience, these equations are rewritten below as Equations 10a to 10d.

$$Y = y_0(\nu/\nu_0) \quad \text{Walsh [10]} \quad (10a)$$

$$Y = Y_0\left[1 - \frac{(10 - 3\nu)(\nu_0 - \nu)}{[10\nu_0 - \nu(1 + 3\nu_0)]}\right]$$

Budiansky and O'Connell [19] (10b)

$$Y = Y_0\left[1 - \frac{(10 - 3\nu_0)(\nu_0 - \nu)}{3(3 - \nu_0)\nu_0}\right]$$

Salganik [17, 18] (10c)

$$Y = Y_0\left[1 + \frac{(10 - 3\nu_0)(\nu_0 - \nu)}{3(3 - \nu_0)\nu}\right]^{-1}$$

Hasselman–Salganik [34] (10d)

For the four models discussed here, Equations 10a to 10d demonstrate that the effect of microcracks on a material's elastic constants can be expressed without explicit knowledge of either the crack number density, N, or the mean crack size $\langle a\rangle$. While each model assumes the existence of a crack population within the material, the researcher is not obliged to provide a value for N (or more properly, the product $N\langle a\rangle^3$, where $\langle a\rangle$ is the mean crack radius) before comparing the theories with experiment. This is important, as there are many complications in estimating N, one of which is the fact that when a specimen is prepared for microscopic examination, by whatever means, the specimen surface is almost invariably damaged. It is difficult to sort out such damage from the inherent crack population. Also, the stress state at the surface of a body is different than in the bulk, so it is not obvious that a statistically meaningful sampling of the cracks will actually intersect the surface. In addition, the fraction of the total population of cracks that appear at the specimen surface may be a function of the microcrack density, the specimen porosity, and perhaps a host of other variables. The same uncertainties in estimating N apply to the estimation of the mean crack radius $\langle a\rangle$; that is, it is difficult to guarantee that one has a statistically valid sampling of the crack sizes existing within the body. These problems may, at least in part, be overcome by small-angle neutron diffraction studies now being done at the National Bureau of Standards [35]. However, there are currently considerable uncertainties involved in experimental values of both N and $\langle a\rangle$, which are thus compounded in the product $N\langle a\rangle^3$.

3.3. Intercomparison of the microcracking–elasticity theories

When expressed in terms of macroscopic variables Y and ν, the predictions of the four microcracking–elasticity models discussed here (Equations 10a to 10d) differ relatively little (Figs. 1a and b). Walsh predicts a linear drop in Y/Y_0, the normalized Young's modulus, as a function of decreasing ν/ν_0, the normalized Poisson's ratio. Each of the three other theories (Budiansky and

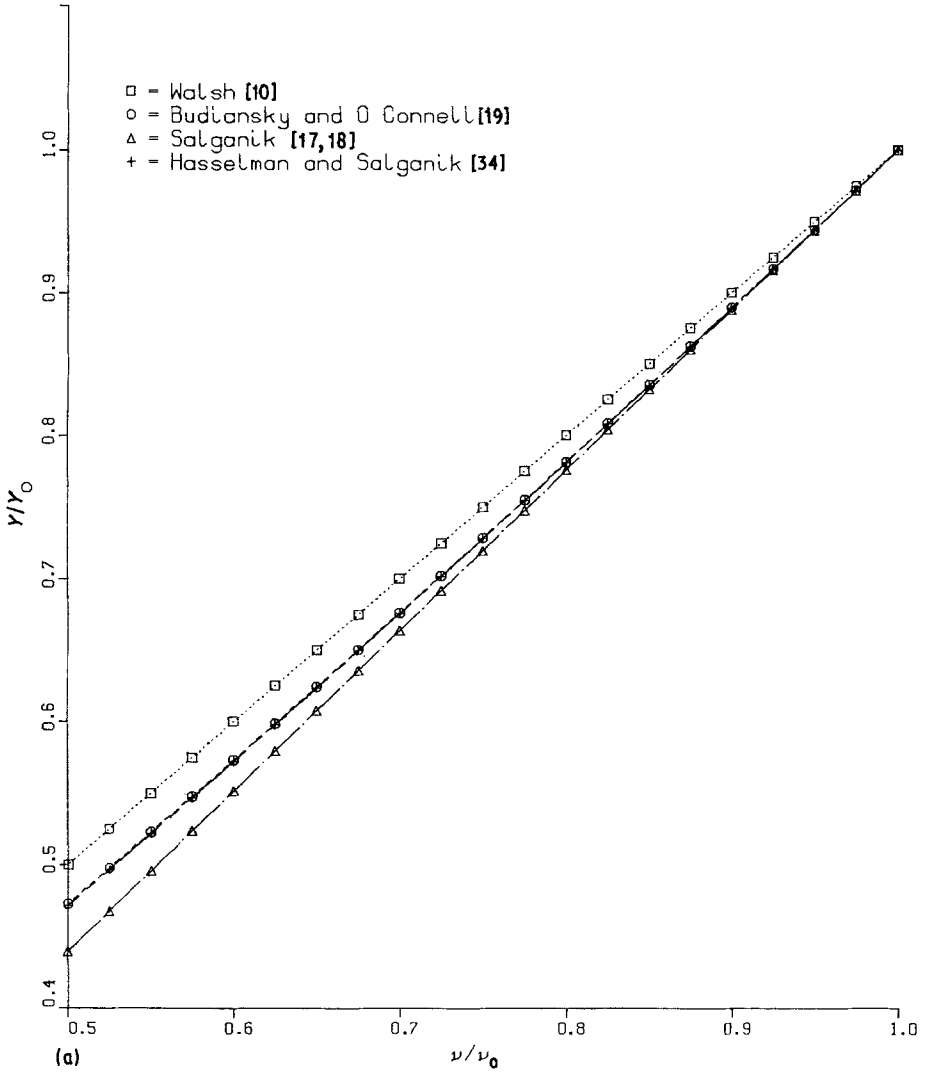

Figure 1 (a) Theoretical predictions of the microcracking–elasticity theories of Walsh, Budiansky and O'Connell, Salganik, and Hasselman–Salganik, as rewritten in terms of normalized Young's modulus, Y/Y_0, and normalized Poisson's ratio, ν/ν_0 (Equations 10a to 10d). (b) Details of the microcracking–elasticity theories for $0.5 \leqslant \nu/\nu_0 \leqslant 1$.

O'Connell, Salganik, and Hasselman–Salganik) yield a nearly linear Young's modulus–Poisson's ratio behaviour that has the Walsh theory as an upper bound over the entire range of ν/ν_0.

It should be noted that Equations 10b to 10d cannot be rewritten explicitly in the form

$$Y/Y_0 = f(\nu/\nu_0),$$

where $f(\nu/\nu_0)$ is a function of ν/ν_0 only. However, if one assigns a particular value to ν_0, then the Y/Y_0 against ν/ν_0 behaviour can be determined. For example, Figs. 1a and b are plotted for the special case of $\nu_0 = 0.25$. Nevertheless, the modulus–Poisson's ratio behaviour is only a very weak function of the magnitude of ν_0. If Figs. 1a and b were replotted for ν_0 anywhere in the range $0.10 \leqslant \nu_0 \leqslant 0.40$ (which includes the ν_0 values of essentially all brittle materials), the replotted figures would, on this scale, be nearly indistinguishable from the present figures. Thus, to a very good approximation, Figs. 1a and b describe the predictions of the four microcracking–elasticity theories, independent of the choice of ν_0.

The modulus–Poisson's ratio predictions of the four microcracking–elasticity theories also show a strict ordering over the entire range of ν/ν_0. If, for convenience, we denote the normalized Young's modulus and Poisson's ratio as

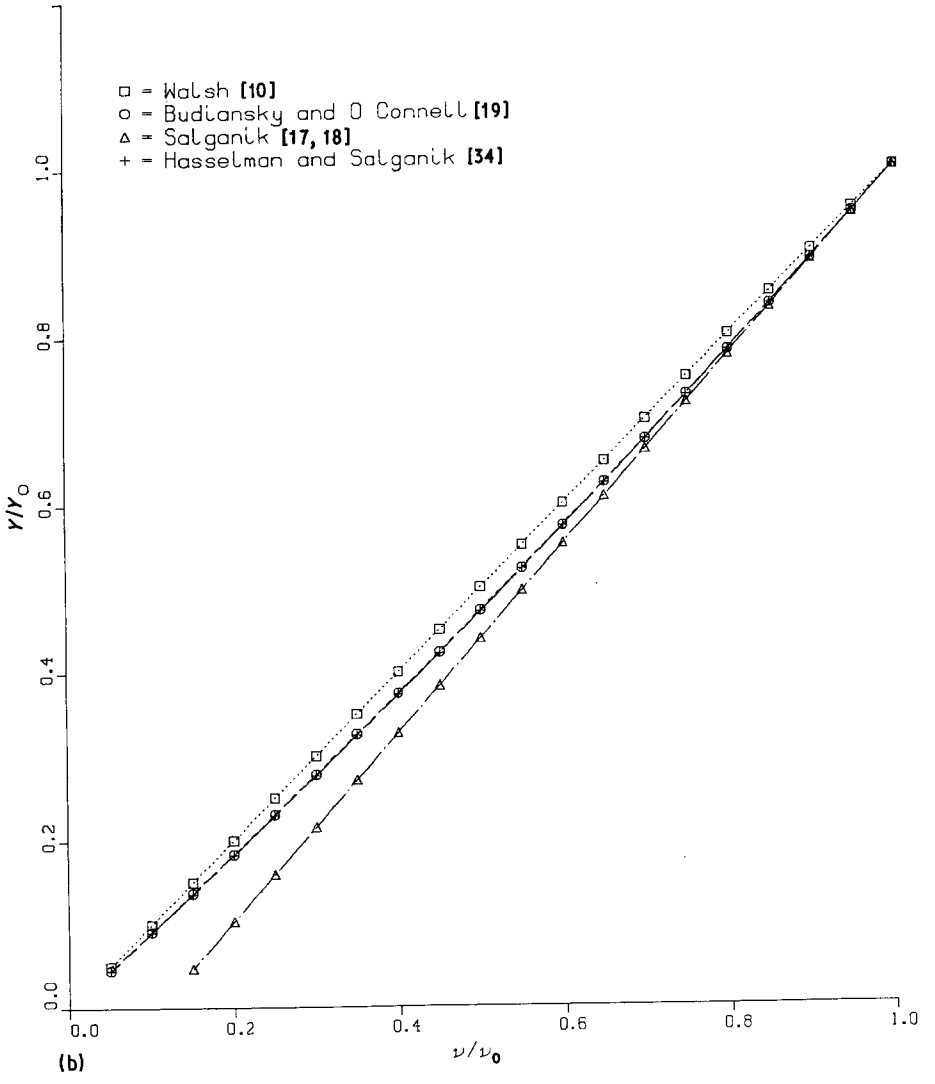

Figure 1 Continued.

$$Y^* = Y/Y_0$$

$$\nu^* = \nu/\nu_0,$$

then the ordering relation may be expressed as

$$Y^*_{\text{Walsh}} > Y^*_{\text{Budiansky and O'Connell}}$$

$$> Y^*_{\text{Hasselman—Salganik}} > Y^*_{\text{Salganik}}$$

for any ν^*, where $0 < \nu^* < 1$. At $\nu^* = 1$ (where $\nu = \nu_0$ and no microcracking has occurred) all theories give $Y^* = 1$.

From Fig. 1, it is also evident that $Y^*_{\text{Budiansky and O'Connell}} \simeq Y^*_{\text{Hasselman—Salganik}}$. For $0.5 \leqslant \nu^* \leqslant 1$, $Y^*_{\text{Budiansky and O'Connell}}$ exceeds $Y^*_{\text{Hasselman—Salganik}}$ by not more than about 0.5%, and for $0.05 \leqslant \nu^* \leqslant 1$, the two theories still agree to within about 1.5%.

Since it does not treat crack interactions, Walsh's linear model applies to quite dilute systems of microcracks, where the number of microcracks per unit volume is small and hence $\nu/\nu_0 \to 1$. However, the Walsh model does offer a surprisingly good approximation of the three other theories, each of which do include crack interaction effects. This demonstrates that crack interaction has a relatively minor effect on Y^*, at least for the theoretical forms presented by Budiansky and O'Connell, Salganik, and Hasselman–Salganik. For each of these three theories the form of the crack interaction, however, is essentially that of a

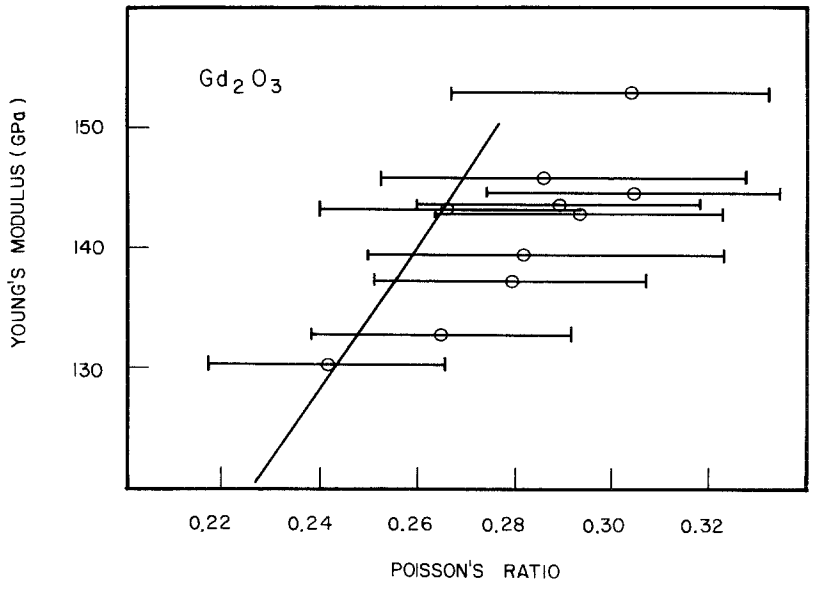

Figure 2 Young's modulus, Y, plotted against Poisson's ratio, ν, for microcracked polycrystalline Gd_2O_3 [22]. Elasticity data represent measurements at room temperature on nine specimens having various grain sizes. The solid curve represents theoretical predictions of the Budiansky and O'Connell equations, written in terms of Y and ν. The error bars represent the ± 10% relative experimental error in determining ν.

first-order perturbation analysis, so that the crack interaction calculations are probably not strictly rigorous for very high number densities of microcracks (that is, for $\nu^* \to 0$).

3.4. Comparison with experiment

In Figs. 2 to 6, the experimental elasticity data for a number of microcracked ceramic oxides are compared to the theoretical curves for the same materials. The data presented here were intentionally selected so that they would represent the following three categories of microcracking–elasticity data: (a) microcracking due to thermal expansion anisotropy, where the elasticity measurements are

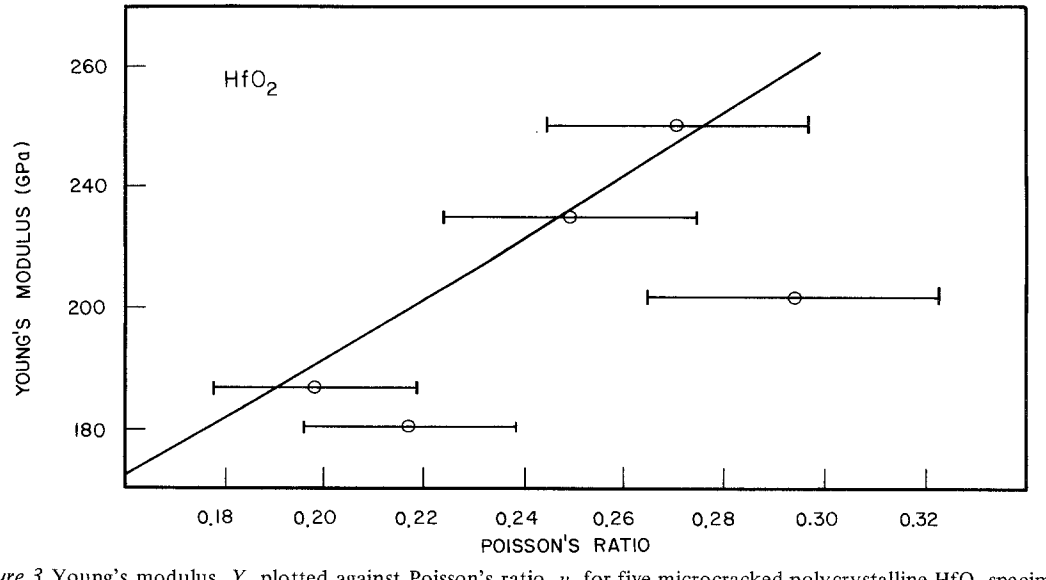

Figure 3 Young's modulus, Y, plotted against Poisson's ratio, ν, for five microcracked polycrystalline HfO_2 specimens, having grain sizes of ~ 2 to 16 μm [24, 25]. The solid curve represents theoretical predictions of the Budiansky and O'Connell equations, written in terms of Y and ν. The error bars represent the ± 10% relative experimental error in determining ν.

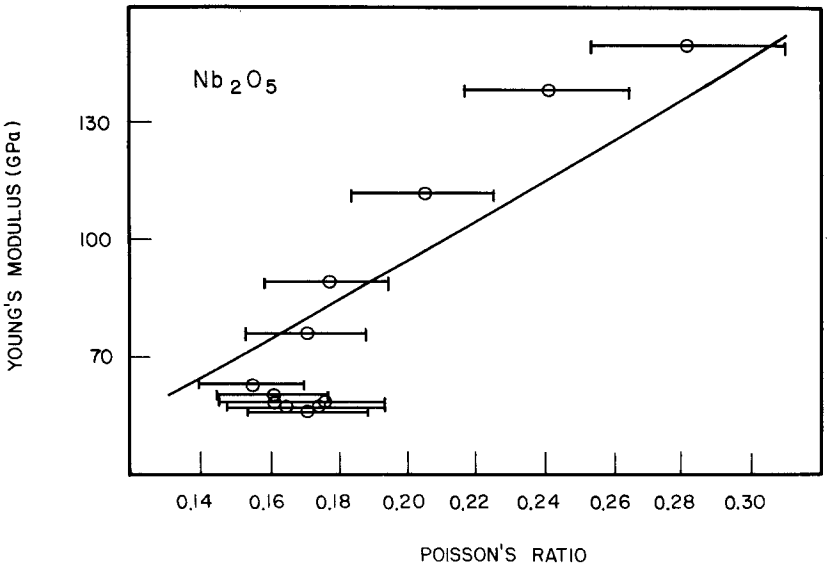

Figure 4 Young's modulus, Y, plotted against Poisson's ratio, ν, for a single microcracked polycrystalline Nb_2O_3 specimen for a single temperature cycle between room temperature and ~ 1050° C [6, 7]. The solid curve represents the theoretical predictions of Budiansky and O'Connell, written in terms of Y and ν. The error bars represent the ± 10% relative experimental error in determining ν.

made as a function of grain size at a fixed temperature; (b) microcracking due to thermal expansion anisotropy, where the elasticity measurements are made as a function of temperature at a fixed grain size; and (c) microcracking due to a phase transformation, where elasticity measurements are performed at room temperature, and the microcrack state of a specimen is controlled through the time and temperature of a thermal anneal.

For all three categories of microcracking data,

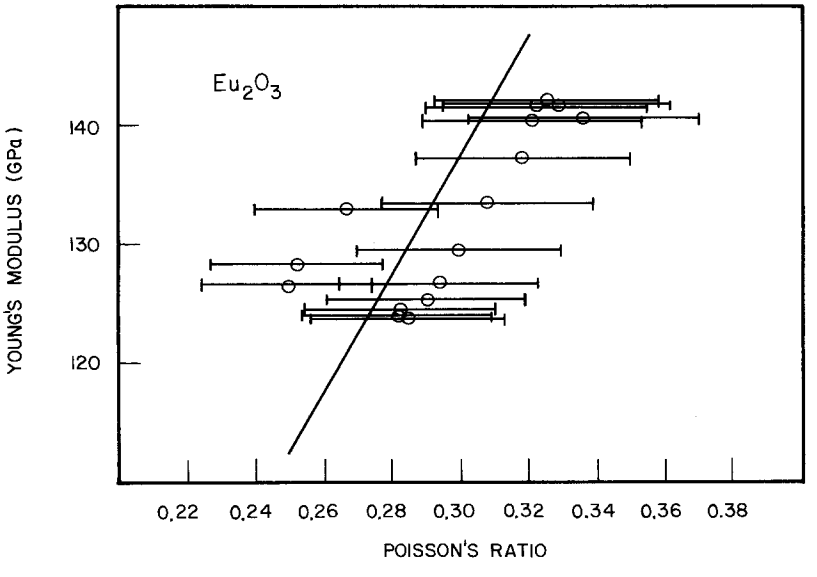

Figure 5 Young's modulus, Y, plotted against Poisson's ratio, ν, for a single polycrystalline, microcracked Eu_2O_3 specimen for a single temperature cycle between room temperature and ~ 1160° C [2]. The solid curve represents the theoretical predictions of Budiansky and O'Connell, written in terms of Y and ν. The error bars represent the ± 10% relative experimental error in determining ν.

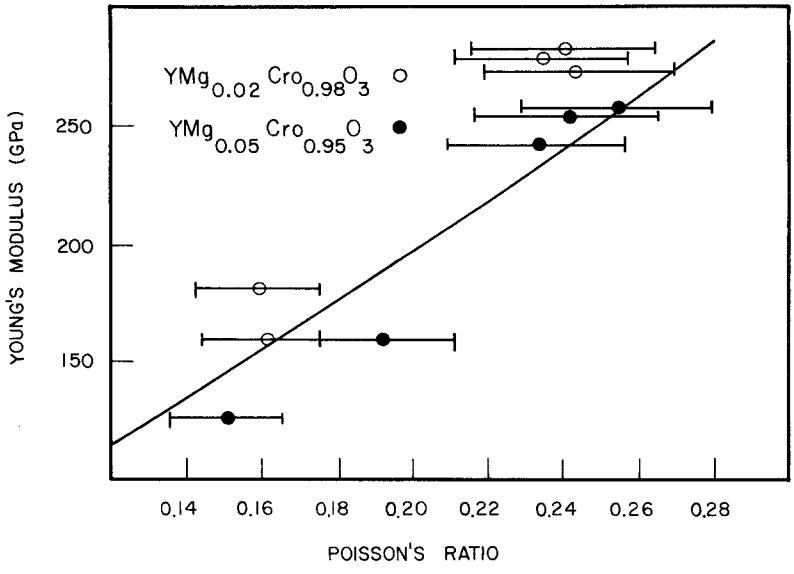

Figure 6 Young's modulus, Y, plotted against Poisson's ratio, ν, for ten polycrystalline, microcracked $YMg_xCr_{1-x}O_3$ specimens [36]. Here the room temperature Y and ν values are varied through thermal anneals above or below the 1100° C phase transition temperature. The solid curve represents the theoretical predictions of Budiansky and O'Connell, written in terms of Y and ν. The error bars represent the ± 10% relative error in determining ν.

the observable, macroscopic parameters Y and ν are plotted‡ (Figs. 2 to 6). In each case, one can view the simultaneous decrease in Y and ν as a result of an increase in the crack number density N, or mean microcrack radius $\langle a \rangle$, although the underlying microscopic parameters N and $\langle a \rangle$ are not explicitly measured nor do they explicitly appear in the rewritten forms of the theories (Equations 10a to 10d, Section 3.2).

The predictions of each of the four theories differ very little, especially over the range of ν^* and Y^* acually seen in the data, so that only the curves corresponding to the predictions of Budiansky and O'Connell are plotted here. For each material, Table I lists the particular Y_0 and ν_0 values used to determine the upper terminus of the theoretically predicted line. A different choice of Y_0 and ν_0 would thus move this upper endpoint, but calculations show that the slope of the predicted line would remain essentially constant for small changes in Y_0 and ν_0. The greater uncertainty involved in determining Poisson's ratio, as compared to Young's modulus, has implications in the correspondence of the theory with the data. (As discussed in the experimental procedure, the experimental uncertainty for the Young's modulus and Poisson's ratio values are ± 1% and ± 10%, respectively.) If the microcracking–elasticity theories are at least approximately correct, then one might expect there to be some probability for the data to be displaced horizontally (in the direction of the ν axis for Figs. 2 to 6) due to the significant uncertainty in ν_0.

3.4.1. Microcrack density as a function of grain size

Figs. 2 and 3 show room temperature elasticity data for HfO_2 [24, 25] and Gd_2O_3 [22] specimens of varying grain size. Both HfO_2 and Gd_2O_3 microcrack due to thermal expansion anisotropy, so that above a critical grain size§, both materials microcrack. Fig. 2 represents a grain size range of ~ 2.3 to 16 μm for the HfO_2 data, and Fig. 3 includes a range of 15.5 to 39 μm for the Gd_2O_3. Although the grain sizes are not explicitly shown (Figs. 2 and 3), each data point in the two figures corresponds to a specimen of a given grain size having a particular Y and ν. For both materials, the highest

‡The Young's modulus and Poisson's ratio was, for all of the data, corrected for volume fraction porosity [4]. Most specimens had volume fraction porosities ⩽ 0.05 [2, 6, 7, 22, 24, 25, 36], so that the magnitude of the porosity correction was not generally large.

§The experimentally determined critical grain size for the onset of microcracking is 2 μm for HfO_2 [24, 25] and 14 μm for Gd_2O_3 [22].

TABLE I Empirically determined values of nonmicrocracked, theoretically dense Young's modulus, Y_0, and Poisson's ratio, ν_0

Material	Y_0 (GPa)	ν_0	Reference
HfO_2	283.6	0.30	[24, 25]
Gd_2O_3	150.3	0.28	[37]
Nb_2O_5	153.4	0.31	[6, 7]
Eu_2O_3	147.7	0.32	[2]
$YMg_xCr_{1-x}O_3$	280.0	0.28	[36]

moduli and Poisson's ratio occur for the smallest grain size, with both Poisson's ratio and modulus decreasing with increasing grain size.

Although all of the Gd_2O_3 specimens (Fig. 2) were sintered, several of the HfO_2 specimens (Fig. 3) were hot pressed. The processing mode may affect the relation between theory and experiment, since each of the four microcracking–elasticity theories discussed here assumes randomly oriented microcracks. These theories are thus applicable to microcracks in polycrystalline bodies having randomly oriented grains. The localized microcracking stresses (due to thermal expansion anisotropy or phase transitions, for example) would presumably result in randomly oriented cracks in polycrystalline materials such as sintered ceramics, where the grains themselves are randomly oriented. Hot-pressed materials, on the other hand, can exhibit some degree of texturing or preferential grain orientation. Microcracks occurring in such materials might also be preferentially oriented, and thus the discrepancy between the data and the theories of Walsh, Budiansky and O'Connell, Salganik, and Hasselman–Salganik should increase as the extent of texturing in a given specimen increases. Thus, possible variations in the degree of texturing due to hot-pressing may be related to at least some of the scatter in the HfO_2 data¶ (Fig. 3).

Analytical expressions do exist for the Young's modulus and Poisson's ratio for bodies having a non-random distribution of microcracks, but such theories typically assume a spatial distribution in which all the microcracks are parallel [20, 21]. This would correspond to an extreme in texturing, analogous to the highly oriented structure of prolytic graphite, for example. A microcracking–elasticity theory appropriate for hot-pressed materials would have to treat the intermediate regime between the two extremes of completely random microcrack orientation and fully parallel microcrack alignment.

Despite possible problems with texturing in the HfO_2 specimens, the data for both Gd_2O_3 and HfO_2 fit the predicted trend reasonably well.

3.4.2. Microcrack density as a function of temperature

Figs. 4 and 5 give elasticity data for Nb_2O_5 [6, 7] and Eu_2O_3 [2], both of which microcrack due to thermal expansion anisotropy*. Thus the microcrack state (and hence Y and ν) for a single specimen can be varied by thermal cycling between room temperature and some elevated temperature. Heating from room temperature heals microcracks at sufficiently high temperatures [4], and subsequent cooling reopens microcracks [4–8].

The healing and reopening of microcracks results in a hysteresis in both the Young's modulus–temperature and the Poisson's ratio–temperature curves [6–8]. The theoretically predicted trends again correspond relatively well to the data for thermally cycled Nb_2O_5 and Eu_2O_3. The apparent systematic shift in the Eu_2O_3 data to the right of the theoretical curve by an additive Poisson's ratio factor of about 0.015 may result from an error in determining ν_0 for Eu_2O_3, since Y_0 and ν_0 determine the upper terminus of the theoretical curve.

3.4.3. Microcrack density as a function of anneal time and temperature

Fig. 6 shows room temperature elasticity data for sintered $YMg_xCr_{1-x}O_3$ (with $x = 0.05$ or 0.02) specimens having a grain size of approximately 6 μm and a volume fraction porosity of ~ 0.05. These specimens microcrack due to an apparent phase transition in the neighbourhood of 1100° C [36]†.

¶The degree of texturing of the hot-pressed HfO_2 specimens was not determined [24, 25].

*Both specimens were sintered. The Nb_2O_5 specimen had a volume fraction porosity of about 0.11 and a grain size of approximately 20 μm [6, 7]. The Eu_2O_3 specimen had a volume fraction porosity of ~ 0.05, and while the average grain size was not determined, the specimen's grain size is presumably above the 8.0 μm critical grain size for Eu_2O_3 [2].

†High-temperature X-ray measurements, differential thermal analysis, and extensive elasticity data all indicate the presence of a phase transition at about 1100° C for $YCrO_3$ and $YMg_xCr_{1-x}O_3$ [36]. Although $YCrO_3$ and $YMg_xCr_{1-x}O_3$ (for $x \leqslant 0.05$) are distorted perovskites at room temperature, the high-temperature crystallographic form has yet to be established. Thus the existence of a high-temperature phase transition at 1100° C must be considered somewhat tentative until the exact high-temperature crystallographic form is documented.

$YMgCr_{1-x}O_3$ sintered in forming gas at about 1700° C shows an anomalously low Young's modulus (i.e. ~120 GPa) in the as-sintered state. Annealing at temperatures in the range of 900 to 1080° C invariably causes the Young's modulus to increase rapidly with time, and then level off at a steady state value of ~260 GPa, while annealing above 1100° C, and subsequently cooling to room temperature always causes the modulus to drop back down to the as-sintered value. By adjusting the time and temperature of the anneal, intermediate microcrack states may be obtained.

Although all of the microcracking theories and data have been presented in terms of the Young's modulus, Y, and Poisson's ratio, ν, equations similar to Equations 10a to 10d can be found relating microcrack behaviour to any pair of the following parameters: Y, ν, G, and B, where B is the bulk modulus and G is the shear modulus [38]. Thus, given the proper data, one could depict the effect of microcracking on a specimen by a plot of Y against G, or B against ν, for example.

4. Conclusions

The results of the microcracking–modulus decrement theories by Walsh, Budiansky and O'Connell, Salganik, and Hasselman–Salganik can all be written in terms of a pair of macroscopic variables (here Young's modulus and Poisson's ratio was used). This eliminates the explicit reference to the mean microcrack radius, $\langle a \rangle$, and the crack number density, N, so that each theory can be expressed in terms of macroscopic, observable quantities.

Elasticity data for several microcracked ceramic oxides were found to be in general agreement with the trends predicted theoretically. The data were selected so that the microcracking state varied as a function of (a) grain size at a fixed temperature, (b) temperature, at a fixed grain size, or (c) time and temperature of anneal. Data types (a) and (b) included materials that microcrack due to thermal expansion anisotropy, while data type (c) is pertinent to materials that undergo a phase transition that induces microcracking. In order to compare with the theoretical predictions of the microcracking–elasticity data, all the data were plotted in terms of Young's modulus to Poisson's ratio.

Each of the four models discussed here give very similar results for the predicted Young's modulus–Poisson's ratio behaviour of a cracked specimen. Walsh predicts a strictly linear dropoff in modulus as a function of Poisson's ratio, while the other three models predict a slightly lower modulus (than does Walsh) for a given Poisson's ratio.

To a very good approximation, the models of Budiansky and O'Connell and of Hasselman–Salganik give identical results over the entire range of Y^*, the normalized Young's modulus, and ν^*, the normalized Poisson's ratio. Each of the four theories, however, must be regarded as only approximate for very high microcrack number densities where both Y^* and ν^* will tend to zero. None of the four theories discussed here treat either second-order crack interaction effects, or (more importantly) microcrack link-up, although both of the effects should probably be included in theories that attempt to deal with very high microcrack densities. The assumptions of the Walsh theory, in particular, are really only appropriate for dilute crack systems ($\nu^* \to 1$), where crack interactions can be ignored. Also, each of the theories (Walsh, Budiansky and O'Connell, Salganik and Hasselman–Salganik) assumes randomly oriented microcracks, so none of these models is likely to be entirely correct for a highly textured material, where the microcracks are preferentially oriented.

Acknowlegements

The authors wishes to thank Dr E. R. Fuller of the Inorganic Materials Division, National Bureau of Standards, Washington, D.C., and Dr R. J. Fields of the Fracture and Deformation Division, National Bureau of Standards, Washington, D.C., for many helpful discussions and for their careful reading of this manuscript. The author also acknowledges the financial support of a National Research Council postdoctoral associateship during the time this work was done at the National Bureau of Standards, Washington, D.C.

References

1. J. J. CLEVELAND and R. C. BRADT, *J. Amer. Ceram. Soc.* **61** (1978) 478.
2. R. R. SUCHOMEL and O. HUNTER Jr, *ibid.* **59** (1976) 149.
3. N. N. AULT and H. F. G. UELTZ, *ibid.* **36** (1953) 199.
4. E. D. CASE, J. R. SMYTH and O. HUNTER Jr, "Fracture Mechanics of Ceramics", Vol. 5, edited by R. C. Bradt, A. G. Evans, D. P. H. Hasselman and F. F. Lange (Plenum Press, New York, 1983) pp. 507–30.
5. J. A. KUSZYK and R. C. BRADT, *J. Amer. Ceram. Soc.* **56** (1973) 420.

6. W. R. MANNING and O. HUNTER Jr, *ibid.* **56** (1973) 602.
7. W. R. MANNING, PhD thesis, Iowa State University, Ames, Iowa (1980).
8. E. D. CASE, PhD thesis, Iowa State University, Ames, Iowa (1980).
9. W. A. ZISMAN, *Proc. Nat. Acad. Sci.* **19** (1933) 653.
10. J. B. WALSH, *J. Geophys. Res.* **70** (1965) 5249.
11. J. H. FILLOUX, *Rev. Geophys. Space Phys.* **17** (1979) 282.
12. W. F. BRACE, *J. Geophys. Res.* **70** (1965) 391.
13. F. BIRCH, *ibid.* **65** (1960) 1083.
14. *Idem, ibid.* **66** (1971) 2199.
15. *Idem, ibid.* **70** (1965) 399.
16. *Idem, ibid.* **70** (1965) 381.
17. R. L. SALGANIK, *Mech. Solids* 8(4) (1973) 135; English translation.
18. *Idem, ibid. Izv. AN. SSSR. Mekhanika Tverdogo Tela* 8 (4) (1973) 149. Original Russian.
19. B. BUDIANSKY and R. J. O'CONNELL, *Int. J. Solids Structures* **12** (1976) 81.
20. D. T. GRIGGS, D. D. JACKSON, L. KNOPOFF and R. L. SHREVE, *Science* **187** (1975) 587.
21. A. HOENIG, *Int. J. Solids Structures* **15** (1979) 137.
22. E. D. CASE, J. R. SMYTH and O. HUNTER Jr, *J. Nuclear Mater.* **102** (1981) 135.
23. *Idem, Mater. Sci. Eng.* **51** (1981) 175.
24. S. L. DOLE, O. HUNTER Jr, F. W. CALDERWOOD and D. J. BRAY, *J. Amer. Ceram. Soc.* **61** (1978) 486.
25. S. L. DOLE, M.S. thesis, Iowa State University, Ames, Iowa (1977).
26. T. NEGAS, Personal communication, Inorganic Materials Division, National Bureau of Standards, Washington, D.C. (1982).
27. M. O. MARLOWE, M.S. thesis, Iowa State University, Ames, Iowa (1963).
28. F. FORSTER, *Z. Metallkde* **29** (1937) 109.
29. S. SPINNER and W. E. TEFFT, *A.S.T.M. Proc.* **61** (1961) 1221.
30. G. PICKETT, *ibid.* **45** (1945) 846.
31. D. P. H. HASSELMAN, "Tables for the Computation of Shear Modulus and Young's Modulus of Rectangular Prisms" (Carborundum Co., Niagara Falls, N.Y., 1961).
32. Annual Book of ASTM Standards, C215-60 (1981).
33. E. SCHREIBER, O. L. ANDERSON and N. SOGA, "Elastic Constants and Their Measurement" (McGraw-Hill, New York, NY, 1974).
34. D. P. H. HASSELMAN and J. P. SINGH, *Ceram. Bull.* **58** (1979) 856.
35. E. D. CASE and C. J. GLINKA, *J. Mater. Sci.* **19** (1984) 2962.
36. E. D. CASE, T. NEGAS, and L. P. DOMINQUES, unpublished data (1982).
37. J. A. HAGLUND and O. HUNTER Jr, *J. Amer. Ceram. Soc.* **56** (1973) 327.
38. E. D. CASE and E. R. FULLER, unpublished work (1983).

Received 16 January
and accepted 24 January 1984